ACS Energy LETTERS

http://pubs.acs.org/journal/aelccp

VIEWPOINT

Lithium Loss in Vacuum Deposited Thin Films

Cite This: *ACS Energy Lett.* 2024, 9, 1753−1758

Read Online

ACCESS | Metrics & More | Article Recommendations | Supporting Information

Thin films serve as ideal model systems for fundamental studies of batteries. Specifically, their very flat surfaces are ideal to probe interfacial phenomena[1−3] and the ability to grow epitaxial films free of grain boundaries enables the study of orientational-dependent electrochemical properties.[4−9] For a wide range of systems, physical vapor deposition (PVD) techniques are the methods of choice for thin film growth, particularly magnetron sputtering for its high-area capabilities which have led to commercialization,[10] and pulsed laser deposition (PLD) for exploratory science owing to its relative ease and potential for stoichiometric transfer of material from target to substrate.[11] However, stoichiometric transfer is not guaranteed for volatile systems, particularly for materials containing lithium. Thus, small changes in the process parameters leads to drastic differences in film composition,[12,13] phase purity (lithium deficient phases are often observed in PVD films[5,14−16]), and consequent film properties.[17,18] Yet, for battery and lithionic applications which utilize thin films, particularly solid-state electrolytes, optimal stoichiometric composition is essential for good electrochemical performance.[19−21]

Lithium loss during deposition is unavoidable. In fact, it has been both theoretically predicted[22] and experimentally observed for vacuum deposition methods. Figure 1a highlights some of the lithium loss mechanisms that occur during vacuum deposition (including during the target preparation).[12,13,23] Notable loss mechanisms are (1) thermal evaporation due to lithium being very volatile, resulting in losses in both the film and target when exposed to high temperatures, (2) high atmospheric sensitivity of the grown films when exposed to ambient air leading to loss of lithium from the film due to the formation of degradation products, and (3) scattering of Li/Li-oxide species in the plasma plume during deposition at higher gas partial pressures resulting in lithium deficiency in the growing film. Analytical modeling (Figure 1b,c) and experimental evidence (Figure 1d) of scattering has been measured in lithium-containing films.[22,24] Lithium has a high scattering probability due to it being lighter than both the background gas (typically O_2) and the other species in the plume (often transition metals with a significantly higher mass). This makes it particularly prone to backscattering, resulting in a wide apex angle plume and a very small area where high Li content is achievable. If this area is smaller than the substrate, or misaligned, homogeneous films cannot be prepared and composition stray will occur across the film. Further, due to the high velocity of the incoming lithium species (evidenced by the faster expansion of plume in Figure 1c), they can rebound from the surface of the substrate and so not be incorporated in the film, resulting in further deficiency.[13,24]

While Figure 1 predominantly focuses on PLD, it should also be noted that these loss mechanisms are equally relevant to other vacuum deposition techniques such as sputtering. Sources of heat will result in thermal loss mechanisms and the presence of gas collisions (e.g., with O_2, N_2, Ar, etc.) will cause a depletion of species in the films due to gas scattering. Also, exposure to the atmosphere (primarily H_2O and O_2) will lead to degradation product formation on the film surface.

In fact, lithium is not the only element prone to compositional stray. For example, $SrRuO_3$, $Sr_3Ru_2O_7$, and Sr_2RuO_4 thin films can be grown from the same stoichiometric $SrRuO_3$ target merely by fine-tuning the PLD processing parameters to account for the volatility of ruthenium.[18] Moreover, to grow stoichiometric $BiFeO_3$ excess bismuth is often added to targets to compensate for bismuth volatility.[25−27] Additionally, sodium excess is often added to Na-containing films (e.g., Na_xCoO_2 and Na_xMnO_2) to account for significant Na vaporization.[28−30] Unlike the aforementioned examples, the challenge for lithium-containing films is that loss occurs through more than one mechanism. Lithium is both very volatile and very prone to gas scattering. Adding excess lithium to the target does not necessarily result in stoichiometric films. Consequently, careful optimization of the process parameters is required in order to grow high-quality stoichiometric films free from lithium-deficient impurity phases, particularly the target stoichiometry (not necessarily the desired film composition) and substrate positioning in the plume.[12,13,23] Additionally, there are more nuanced parameters/phenomena specific to the given PVD technique that must be considered. See the following reviews that cover these aspects in detail: PLD,[12,13,23] sputtering[31,32] and molecular beam epitaxy.[33]

Lithium loss manifests differently for different phases, examples of which are presented in Figure 2. For $LiCoO_2$ (LCO) lithium loss results in the formation of Co_3O_4 (Figure 2a,b), which does not lithiate in the LCO voltage window (3.7−4.2 V).[34] Therefore, LCO films with significant Co_3O_4 impurities will exhibit diminished areal/specific discharge

Received: January 15, 2024
Accepted: March 12, 2024
Published: March 26, 2024

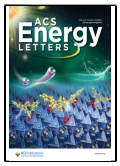

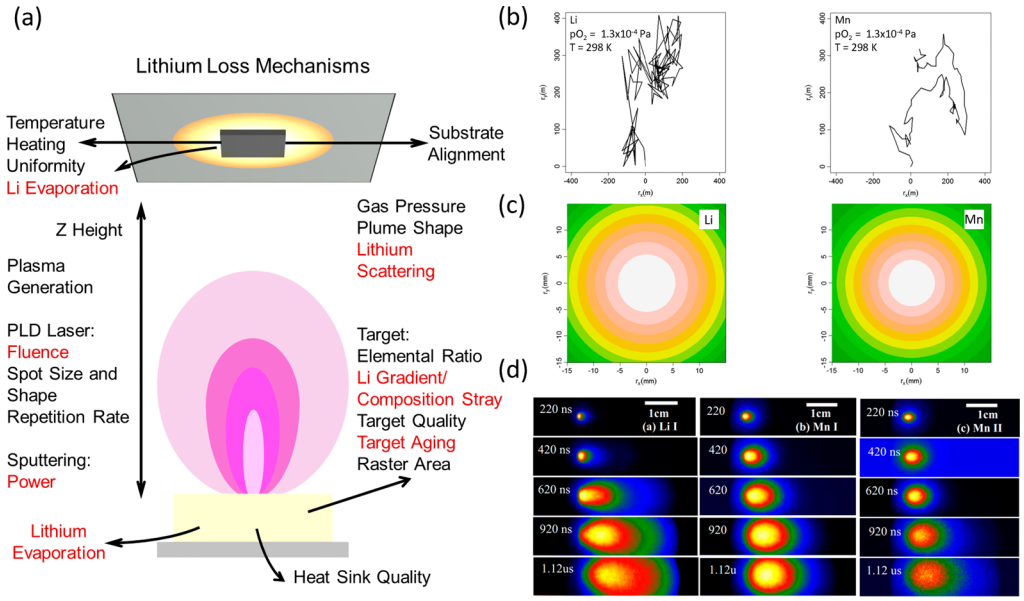

Figure 1. Origins of lithium loss during vacuum deposition. (a) Schematic of plasma generated during vacuum deposition highlighting process parameters and mechanisms that can influence the lithium stoichiometry of the thin film. Processes where direct loss of lithium can occur are highlighted in red. (b) and (c) Theoretical and (d) experimental evidence of lithium scattering during pulsed laser deposition (PLD) of $LiMn_2O_4$ films. (b) Trajectory simulations of stochastic scattering of Li and Mn at $pO_2 = 10^{-6}$ Torr and $T = 298$ K. Lithium is scattered more violently than manganese and undergoes significant backscattering, constituting to lithium deficiency. (c) Simulated probability density plots for Li and Mn during PLD ($pO_2 = 1.3$ Pa, $T = 298$ K, expansion after 5 μs with v = 10^2 m s^{-1}, a typical average velocity for ablated atoms[58] (0.05 mm Z height)). Li scatters over a wider area than Mn. Reproduced with permission from ref 22. Copyright 2013 American Physical Society. (d) Space and time-resolved emission spectroscopy of a $LiMn_2O_4$ PLD plume. The plume dynamics are clearly different for Li and Mn, with increased angular broadening of the plume observed for Li I. This is a direct consequence of scattering and demonstrates the importance of optimizing the deposition pressure and Z height. Reproduced with permission from ref 24. Copyright 2009 AIP Publishing.

capacities.[19,35] Further, lowered lithium content in LCO can lead to the formation of nonstoichiometric two-phase (hexagonal and monoclinic) films, as detected during electrochemical testing (Figure 2c).[36] This can impair electrochemical performance, due to nonuniform volume changes causing microcracking, which results in increased capacity fade.[37] For $LiMn_2O_4$ (LMO), Mn_2O_3 and Mn_3O_4 are often detected (Figure 2d).[5,38−40] Again, films with high MnO_x content will exhibit lowered areal/specific discharge capacities. Epitaxial films of different orientation show different tendencies to form manganese oxide impurity phases, with the (001) orientation being more prone ascribed to preferential alignment of the fast Li^+ conduction channels abetting volatility.[5] If the growth temperature is too high (>∼650 °C), lithium can be completely driven off resulting in the spinel LMO phase not forming.[41] Conversely, if the growth temperature is significantly lowered, this can result in the formation of lithium-rich LMO, including $Li_2Mn_2O_4$, compensating for volatility issues.[42]

For the solid-state electrolytes $Li_{3x}La_{2/3-x}TiO_3$ (LLTO) and $Li_7La_3Zr_2O_{12}$ (LLZO), lowered Li^+ ionic conductivity, typically 2−3 orders of magnitude lower in thin films vs bulk, is often reported and ascribed to lithium loss (Figure 2e,f).[36,43,44] The reduced conductivity arises due to a net loss of Li^+ charge carriers during deposition, exacerbated by volatile loss mechanisms due to the very high growth temperatures required for high crystallinity (often >800 °C). Further, Li deficient phases are also often detected in LLTO and LLZO, which likely impede performance. TiO_2,[14,45,46] $La_2Ti_2O_7$,[14,45,47] and spinel $Li_4Ti_5O_{12}$[6,47] are commonly reported in LLTO films. For LLZO, the Li-deficient phase $La_2Zr_2O_7$ is often observed, impacting Li^+ transport, reducing the ionic conductivity and raising the activation energy.[12,15,48] Further, the high reactivity of LLZO toward CO_2 leads to Li_2CO_3 formation on the film surface, increasing the interfacial resistance when implimented in solid-state batteries.[43] It should also be noted that Li-deficient impurity phases are often detected in thicker films (>100 nm) but are less common in thinner films (<100 nm). Li-deficient impurity phases may be equally prevalent in thinner films owing to the difficulty in resolving X-ray diffraction (XRD) reflections in thinner films.[6]

A number of approaches have been employed to compensate for lithium loss in thin films during deposition including: adding excess lithium to the PLD target, typically between 5 and 20 wt % of lithium;[5,6,14] growth of superlattice films with alternating layers of the phase to be studied and a lithium-rich phase, e.g., Li_2O or Li_3N, to supply lithium to the film of interest;[44,49] codepositing with a lithium-rich phase;[50] or post-annealing in lithium-rich atmospheres to reintroduce lithium to the as-grown film.[15] While these approaches help maintain higher lithium content in the said films, there is no fine control of the lithium incorporation, and in some cases the approaches produce unwanted microstructural defects, such as voids within the superlattice film due to collapse of the sacrificial lithium-rich layers.[51] Therefore, there is still no guarantee that either the targeted lithium stoichiometry is achieved or that unwanted secondary phases will not form. In fact, Li-deficient MnO_x phases are detected in LMO thin films with 100 wt % excess of Li.[5] Thus, if the film stoichiometry cannot be carefully controlled, the electrochemical performance will vary from point to point across the sample, which is potentially detrimental to the overall performance of the film.

https://doi.org/10.1021/acsenergylett.4c00153
ACS Energy Lett. 2024, 9, 1753−1758

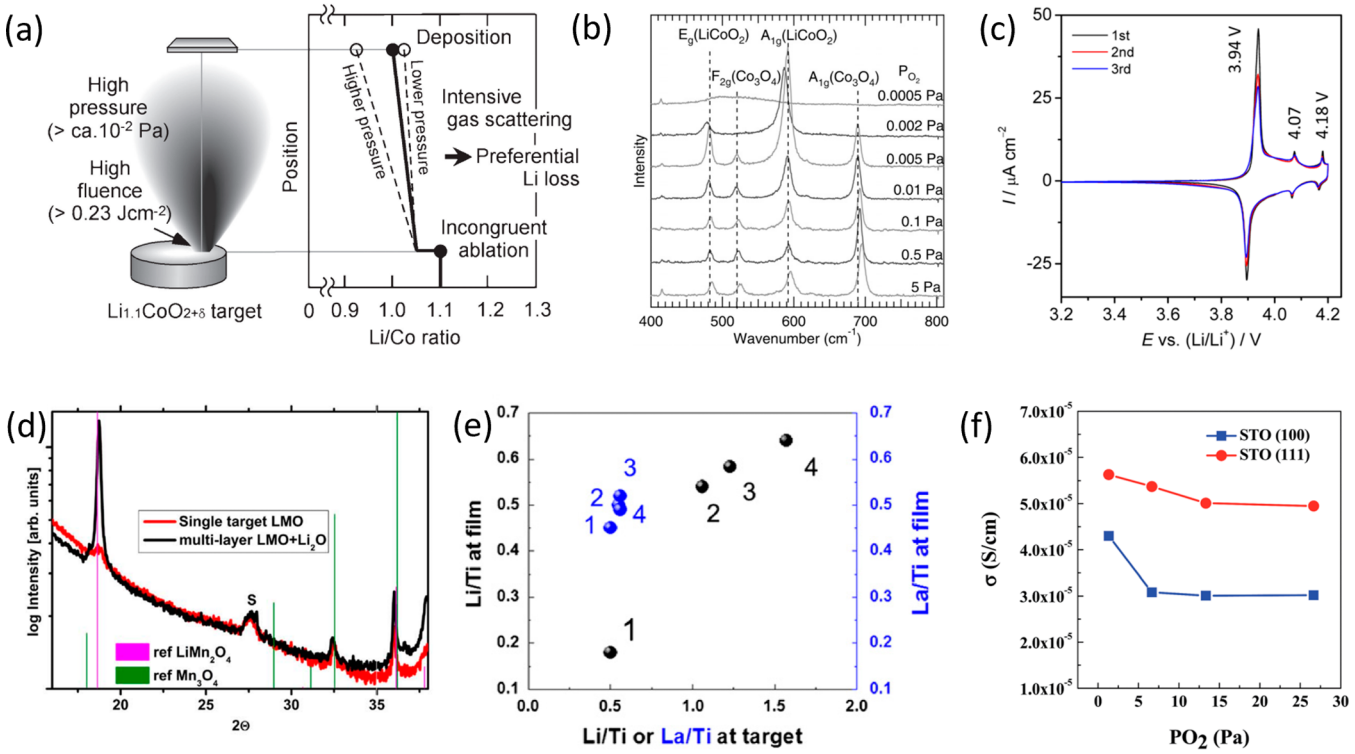

Figure 2. Macroscale evidence of lithium loss in PLD battery thin films. (a) Schematic and (b) Raman spectroscopy evidence of compositional deviation in Li-rich $LiCoO_2$ target. Increasing the pO_2 during growth intensifies Li gas scattering, resulting in an enhanced Co_3O_4 Raman signal. Reproduced with permission from ref 35, copyright 2012 IOP Publishing, and ref 19, copyright 2010 Springer Nature. (c) Cyclic voltammogram of LCO/SRO/STO (111) film cycled with an upper cutoff voltage of 4.2 V (corresponding to Li_xCoO_2, $x > 0.5$). Three redox peaks are present: the major 3.94 V peak corresponds to a first-order metal−insulator transition, and the two minor peaks correspond to the order−disorder transitions around $Li_{0.5}CoO_2$.[59,60] Observation of the minor redox peaks in the first cycle is indicative of the presence of LCO, with $x < 0.5$. Reproduced with permission from ref 21. Copyright 2015 American Chemical Society. (d) XRD pattern of LMO thin films, with reflections marked in green corresponding to Li deficient impurity phase Mn_3O_4. Reproduced with permission from ref 40. Copyright 2018 Elsevier. (e) Measured composition and (f) ionic conductivity of LLTO thin films. In (e), the Li/Ti ratio of the target is not retained in the film, even when significant excess of Li is added. This impacts the measured ionic conductivity (f). First, all films exhibit 2 orders of magnitude lower ionic conductivity than bulk (10^{-3} S cm^{-1}).[61] Further reduction in conductivity occurs with increasing pO_2 due to Li scattering. Reproduced from ref 36 with permission. Copyright 2016 Royal Society of Chemistry.

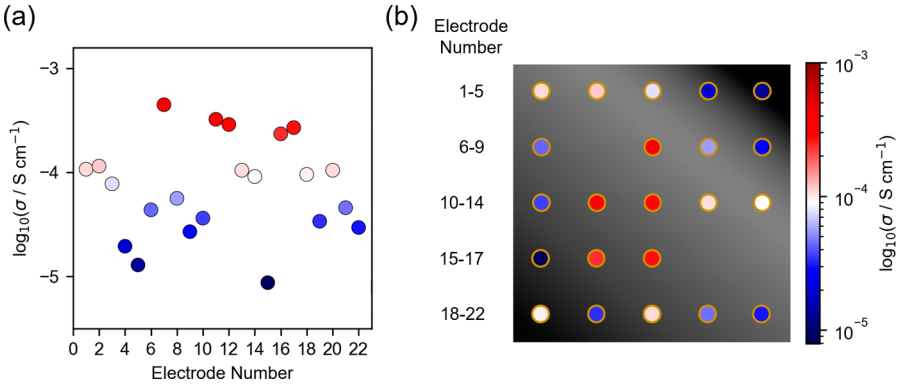

Figure 3. Microscale evidence of lithium loss studied with local ionic conductivity measurements. (a) magnitude of Li^+ ionic conductivities calculated from 22 gold microdot electrodes (300 μm in diameter). (b) Spatial location of the electrodes where the colors corresponds to the magnitude of ionic conductivity. See the Supporting Information for an extended figure.

As highlighted, the majority of studies focus on macroscale (thus the average) composition of the film (Figure 2). However, normally macroscopic in-plane measurements are made using large area (>1 mm^2) square/bar electrodes and so average (rather than local) film properties are measured.[6,14,15,20,44] Hence, there is no information on the variation of properties across the film area. Considering the high potential for lithium variability across Li-based thin films, it is important to be able to understand the local properties point-to-point across a sample. This is particularly important when long-range homogeneous performance is vital, such as lithionic devices for neuromorphic computing.

Instead, we utilize the microdot approach to measure the *local* Li^+ ionic conductivity (out-of-plane geometry) across the

https://doi.org/10.1021/acsenergylett.4c00153
ACS Energy Lett. 2024, 9, 1753−1758

total area of a $Li_xLa_{0.32}Nb_{0.7}Ti_{0.3}O_3$-based (LL(Nb,Ti)O) film (22 discrete gold microdot electrodes with 0.07 mm^2 area). This system was chosen for its sizable Li^+ ion conductivity, up to 10^{-4} S cm^{-1} at 25 °C.[52] Please refer to Supporting Information Note 1 for an extended discussion. Across the film, a 2 orders of magnitude distribution in Li^+ ion conductivity is observed (10^{-6}–10^{-4} S cm^{-1}, Figure 3a). Considering the spatial distribution of the electrodes (Figure 3b), we note that the highest ionic conductivities tend to be observed at the center of the film, whereas lower ionic conductivities are located at the peripheries. The large variations in ionic conductivity across the film are understood by considering how the PLD parameters and plume dynamics influence lithium stoichiometry (recall Figure 1). Specifically, lithium is more strongly gas-scattered than heavier species (Ti, La, and Nb), resulting in deviations from the stoichiometric ratio in a concentric way from the center of the PLD plume,[22,24] as discussed earlier. Further, titanium is also prone to severe gas scattering, which can result in deviations from the desired Ti:La ratio.[6] It is noted that, for LLTO, there is a strong relationship between ionic conductivity and lithium content, displaying a parabola-type relationship with a maxima in ionic conductivity (~10^{-3} S cm^{-1}) at $Li_{3x}La_{2/3-x}TiO_3$, x = 0.067.[53,54] This parabola-type trend is also observed in doped LLTO.[55,56] The ionic conductivity can deviate by 1–2 orders of magnitude with a small deviations in the composition.[53]

It should be stressed that the observations in Figure 3 are not unexpected. Our work highlights that this phenomenon can occur on a *local* scale, point-to-point across the sample, and that lithium-containing films are particularly prone to deviations. This has potentially detrimental consequences for the electrochemical performance of the film which warrants consideration.

We emphasize here that, like many other studies,[5,6,14] we added excess lithium to our PLD target to combat lithium loss (10 wt % excess Li_2O). And yet, through spatially mapping the ionic conductivity of our film we observe clear inhomogeneity in ionic conductivity across the sample (Figure 3). Our results have implications for the wider thin film battery and lithionics fields. First, our results demonstrate that adding excess lithium to PLD targets does not necessarily eliminate lithium loss on a *local* scale. Hence, sample inhomogeneity may be an intrinsic property not accounted for in many lithium-containing PLD films. Second, macroscale electrochemical impedance spectroscopy (EIS) measurements utilizing bar electrodes that measure the *average* performance by probing large regions of the sample (e.g., using bar electrodes) disguise *local* inhomogeneities. This may account for why many PLD grown LLTO planar films exhibit lower-than-expected Li^+ ionic conductivity.[6,14,57] Finally, our results validate the need to map the local properties of lithium-containing thin films, so that "*more averaged*" measurements can be contextualized. This is particularly relevant when comparative macroscale measurements are undertaken (i.e., measuring the properties of a film exposed to a stimulus and comparing it with a reference sample) such that inhomogeneities are accounted for. Crucially, a greater understanding of the film on a *local* scale will improve the macroscale performance and thus overall quality of the resultant film.

As a final remark, it is worth considering when and where lithium loss poses the most significant problems. With a well-optimized PVD growth, it is possible to mitigate against lithium loss entirely, the complexity of which ultimately depends on the technique chosen and the desired characteristics of the film. For example, an amorphous/polycrystalline film of a tertiary system (e.g., Li, O + 1 other element) grown at low/room temperature is less likely to be impacted by lithium loss than an epitaxial complex oxide containing many elements grown at high temperature (>500 °C). Naturally, there will be film-systems/PVD growth conditions where lithium loss is not as significant. Nonetheless, the challenges highlighted within our viewpoint still need to be considered and overcome. Finally, the material grown and its intended purpose will also factor into the impact that lithium loss has. For batteries, negative electrodes are unlikely to present problems, as the majority are grown in their delithiated state (e.g., Si, C, TiO_2, Nb_2O_5, etc.).[12] Solid electrolytes are particularly prone as the loss of charge carriers will result in lowered ionic conductivity and a tendency to form Li-deficient impurity phases. Both are very detrimental to performance and will lead to inhomogeneous performance, thus careful optimization of processing parameters is essential, particularly the target composition (not necessarily the desired film composition) and the substrate positioning in the plume.[13] For positive electrodes such as $LiMn_2O_4$, $LiCoO_2$, and $LiNi_{1-x-y}Mn_xCo_yO_2$ (NMC) (and lithium-containing negative electrodes like $Li_4Ti_5O_{12}$), it really depends on the cycling conditions and final application. If the film is to be cycled in an environment where excess lithium is present, e.g., half-cell vs Li metal in liquid electrolyte, with suitable voltage cut-offs that enable full lithiation, low-level lithium deficiencies are unlikely to be detrimental provided it does not hinder the formation of the phase. This is because the film can relithiate during cycling. However, if lithium cannot be reintroduced to the film, or there is a small lithium reserve (e.g., in a solid-state battery), then lithium loss can pose significant performance limitations due to Li-deficient phase formation, strongly limiting the achievable current density and total areal/specific capacity of the film.

To summarize, from a survey of current literature, this Viewpoint identifies and discusses lithium loss mechanisms during vacuum deposition methods. Next, by spatially mapping variations in Li^+ ionic conductivity across LL(Nb,Ti)O-based thin films, we found the Li^+ ionic conductivity varies by 2 orders of magnitude across the total film area (25 mm^2). This large variation is attributed to severe gas scattering of light lithium species during deposition. This result demonstrates that large variable local performance is present, an intrinsic property in many films which will not be detected by commonly undertaken macroscale measurements. This work highlights the need to investigate local performance variation arising from lithium nonstoichiometry which is prevalent in vacuum grown thin films.

Adam J. Lovett orcid.org/0000-0002-3076-2992
Ahmed Kursumovic
Judith L. MacManus-Driscoll orcid.org/0000-0003-4987-6620

■ ASSOCIATED CONTENT

Supporting Information

The Supporting Information is available free of charge at https://pubs.acs.org/doi/10.1021/acsenergylett.4c00153.

Experimental section and extended discussion of spatial mapping of Li^+ ionic conductivity in LL(Nb,Ti)O-based

https://doi.org/10.1021/acsenergylett.4c00153
ACS Energy Lett. 2024, 9, 1753−1758

thin film (microstructure, schematic and cross-sectional TEM; EIS, Nyquist plots) (PDF)

AUTHOR INFORMATION

Complete contact information is available at:
https://pubs.acs.org/10.1021/acsenergylett.4c00153

Notes

Views expressed in this Viewpoint are those of the authors and not necessarily the views of the ACS.
The authors declare no competing financial interest.

ACKNOWLEDGMENTS

J.L.M.-D. acknowledges the ERC advanced grant, EU-H2020-ERC-ADG No. 882929, EROS, and the Royal Academy of Engineering under Grant No. CIET1819_24. A.J.L. acknowledges support from EPSRC (EP/R513180/1). A.J.L., J.L.M.-D., and A.K. acknowledge the EPSRC CAM-IES, Grant No. EP/P007767, for PLD time. J.L.M.-D. and A.J.L. also acknowledge the EPSRC Faraday under Grant No. EP/T005394/1, FutureCat. This work was supported by the Henry Royce Institute for advanced materials through the Equipment Access Scheme enabling access to the Ambient Processing Cluster Tool at Cambridge; Cambridge Royce facilities grant EP/P024947/1 and Sir Henry Royce Institute recurrent grant EP/R00661X/1 A.K. and J.L.M.-D. acknowledge the Leverhulme trust grant RPG-2020-041.

REFERENCES

(1) Swallow, J. E. N.; Fraser, M. W.; Kneusels, N. J. H.; Charlton, J. F.; Sole, C. G.; Phelan, C. M. E.; Björklund, E.; Bencok, P.; Escudero, C.; Pérez-Dieste, V.; Grey, C. P.; Nicholls, R. J.; Weatherup, R. S. Revealing Solid Electrolyte Interphase Formation through Interface-Sensitive Operando X-Ray Absorption Spectroscopy. *Nat. Commun.* **2022**, *13* (1), 6070.
(2) Kumar, R.; Tokranov, A.; Sheldon, B. W.; Xiao, X.; Huang, Z.; Li, C.; Mueller, T. In Situ and Operando Investigations of Failure Mechanisms of the Solid Electrolyte Interphase on Silicon Electrodes. *ACS Energy Lett.* **2016**, *1* (4), 689−697.
(3) Hirayama, M.; Sonoyama, N.; Ito, M.; Minoura, M.; Mori, D.; Yamada, A.; Tamura, K.; Mizuki, J.; Kanno, R. Characterization of Electrode/Electrolyte Interface with X-Ray Reflectometry and Epitaxial-Film $LiMn_2O_4$ Electrode. *J. Electrochem. Soc.* **2007**, *154* (11), A1065.
(4) Suzuki, K.; Hirayama, M.; Kim, K.; Taminato, S.; Tamura, K.; Son, J.-Y.; Mizuki, J.; Kanno, R. Interfacial Analysis of Surface-Coated $LiMn_2O_4$ Epitaxial Thin Film Electrode for Lithium Batteries. *J. Electrochem. Soc.* **2015**, *162* (13), A7083−A7090.
(5) Hendriks, R.; Cunha, D. M.; Singh, D. P.; Huijben, M. Enhanced Lithium Transport by Control of Crystal Orientation in Spinel $LiMn_2O_4$ Thin Film Cathodes. *ACS Appl. energy Mater.* **2018**, *1* (12), 7046−7051.
(6) Ohnishi, T.; Mitsuishi, K.; Nishio, K.; Takada, K. Epitaxy of $Li_{3x}La_{2/3-x}TiO_3$ Films and the Influence of La Ordering on Li-Ion Conduction. *Chem. Mater.* **2015**, *27* (4), 1233−1241.
(7) Li, Z.; Yasui, S.; Takeuchi, S.; Creuziger, A.; Maruyama, S.; Herzing, A. A.; Takeuchi, I.; Bendersky, L. A. Structural Study of Epitaxial $LiCoO_2$ Films Grown by Pulsed Laser Deposition on Single Crystal $SrTiO_3$ Substrates. *Thin Solid Films* **2016**, *612*, 472−482.
(8) Lee, S.; Kim, H.; Lee, J. H.; Kim, B. K.; Shin, H.; Kim, J.; Park, S. Nano-Interface Engineering in All-Solid-State Lithium Metal Batteries: Tailoring Exposed Crystal Facets of Epitaxially Grown $LiNi_{0.5}Mn_{1.5}O_4$ Films. *Nano Energy* **2021**, *79* (May 2020), No. 105480.
(9) KC, B.; Guo, J.; Farrell, J.; Nolis, G. M.; Buchholz, D. B.; Evmenenko, G.; Cabana, J.; Crabtree, G. W.; Klie, R. F. Molecular Beam Epitaxy (MBE) Growth of Model Cathodes to Study Interfacial Ion Diffusion. *Adv. Mater. Interfaces* **2022**, *9* (30), 2201187.
(10) Dudney, N. J. Thin Film Micro-Batteries. *Electrochem. Soc. Interface* **2008**, *17* (3), 44−48.
(11) MacManus-Driscoll, J. L.; Wells, M. P.; Yun, C.; Lee, J. W.; Eom, C. B.; Schlom, D. G. New Approaches for Achieving More Perfect Transition Metal Oxide Thin Films. *APL Mater.* **2020**, *8* (4), No. 040904.
(12) Indrizzi, L.; Ohannessian, N.; Pergolesi, D.; Lippert, T.; Gilardi, E. Pulsed Laser Deposition as a Tool for the Development of All Solid-State Microbatteries. *Helv. Chim. Acta* **2021**, *104* (2), e2000203.
(13) Ojeda-G-P, A.; Döbeli, M.; Lippert, T. Influence of Plume Properties on Thin Film Composition in Pulsed Laser Deposition. *Adv. Mater. Interfaces* **2018**, *5* (18), 1−16.
(14) Aguesse, F.; Roddatis, V.; Roqueta, J.; Garcia, P.; Pergolesi, D.; Santiso, J.; Kilner, J. A. Microstructure and Ionic Conductivity of LLTO Thin Films: Influence of Different Substrates and Excess Lithium in the Target. *Solid State Ionics* **2015**, *272*, 1−8.
(15) Rawlence, M.; Garbayo, I.; Buecheler, S.; Rupp, J. L. M. On the Chemical Stability of Post-Lithiated Garnet Al-Stabilized $Li_7La_3Zr_2O_{12}$ Solid State Electrolyte Thin Films. *Nanoscale* **2016**, *8* (31), 14746−14753.
(16) Loho, C.; Djenadic, R.; Bruns, M.; Clemens, O.; Hahn, H. Garnet-Type Li 7 La 3 Zr 2 O 12 Solid Electrolyte Thin Films Grown by CO_2 -Laser Assisted CVD for All-Solid-State Batteries. *J. Electrochem. Soc.* **2017**, *164* (1), A6131−A6139.
(17) Kumatani, A.; Ohsawa, T.; Shimizu, R.; Takagi, Y.; Shiraki, S.; Hitosugi, T. Growth Processes of Lithium Titanate Thin Films Deposited by Using Pulsed Laser Deposition. *Appl. Phys. Lett.* **2012**, *101* (12), 1−5.
(18) Ohnishi, T.; Takada, K. Epitaxial Thin-Film Growth of $SrRuO_3$, $Sr_3Ru_2O_7$, and Sr_2RuO_4 from a $SrRuO_3$ Target by Pulsed Laser Deposition. *Appl. Phys. Express* **2011**, *4* (2), 025501.
(19) Ohnishi, T.; Hang, B. T.; Xu, X.; Osada, M.; Takada, K. Quality Control of Epitaxial $LiCoO_2$ Thin Films Grown by Pulsed Laser Deposition. *J. Mater. Res.* **2010**, *25* (10), 1886−1889.
(20) Ohnishi, T.; Takada, K. Synthesis and Orientation Control of Li-Ion Conducting Epitaxial $Li_{0.33}La_{0.56}TiO_3$ Solid Electrolyte Thin Films by Pulsed Laser Deposition. *Solid State Ionics* **2012**, *228*, 80−82.
(21) Takeuchi, S.; Tan, H.; Bharathi, K. K.; Stafford, G. R.; Shin, J.; Yasui, S.; Takeuchi, I.; Bendersky, L. A. Epitaxial $LiCoO_2$ Films as a Model System for Fundamental Electrochemical Studies of Positive Electrodes. *ACS Appl. Mater. Interfaces* **2015**, *7* (15), 7901−7911.
(22) Packwood, D. M.; Shiraki, S.; Hitosugi, T. Effects of Atomic Collisions on the Stoichiometry of Thin Films Prepared by Pulsed Laser Deposition. *Phys. Rev. Lett.* **2013**, *111* (3), 1−5.
(23) Ojeda-G-P, A.; Schneider, C. W.; Lippert, T.; Wokaun, A. Pressure and Temperature Dependence of the Laser-Induced Plasma Plume Dynamics. *J. Appl. Phys.* **2016**, *120* (22), 225301.
(24) Canulescu, S.; Papadopoulou, E. L.; Anglos, D.; Lippert, T.; Schneider, C. W.; Wokaun, A. Mechanisms of the Laser Plume Expansion during the Ablation of $LiMn_2O_4$. *J. Appl. Phys.* **2009**, *105* (6), 063107.
(25) Zhu, J.; Luo, W. B.; Li, Y. R. Growth and Properties of $BiFeO_3$ Thin Films Deposited on $LaNiO_3$ -Buffered $SrTiO_3$ (0 0 1) and (1 1 1) Substrates by PLD. *Appl. Surf. Sci.* **2008**, *255* (5), 3466−3469.
(26) Singh, A.; Khan, Z. R.; Vilarinho, P. M.; Gupta, V.; Katiyar, R. S. Influence of Thickness on Optical and Structural Properties of $BiFeO_3$ Thin Films: PLD Grown. *Mater. Res. Bull.* **2014**, *49* (1), 531−536.
(27) Li, Y.; Sritharan, T.; Zhang, S.; He, X.; Liu, Y.; Chen, T. Multiferroic Properties of Sputtered $BiFeO_3$ Thin Films. *Appl. Phys. Lett.* **2008**, *92* (13), 2−5.
(28) Shibata, T.; Fukuzumi, Y.; Kobayashi, W.; Moritomo, Y. Fast Discharge Process of Layered Cobalt Oxides Due to High Na^+ Diffusion. *Sci. Rep.* **2015**, *5*, 8−11.

(29) Zhou, H.; Zhang, X. P.; Xie, B. T.; Xiao, Y. S.; Yang, C. X.; He, Y. J.; Zhao, Y. G. Fabrication of Na_xCoO_2 Thin Films by Pulsed Laser Deposition. *Thin Solid Films* **2006**, *497* (1−2), 338−340.
(30) Katayama, S.; Katase, T.; Tohei, T.; Feng, B.; Ikuhara, Y.; Ohta, H. Reactive Solid-Phase Epitaxy and Electrical Conductivity of Layered Sodium Manganese Oxide Films. *Cryst. Growth Des.* **2017**, *17* (4), 1849−1853.
(31) Ma, Y.; Li, L.; Qian, J.; Qu, W.; Luo, R.; Wu, F.; Chen, R. Materials and Structure Engineering by Magnetron Sputtering for Advanced Lithium Batteries. *Energy Storage Mater.* **2021**, *39* (March), 203−224.
(32) Kelly, P. J.; Arnell, R. D. Magnetron Sputtering: A Review of Recent Developments and Applications. *Vacuum* **2000**, *56* (3), 159−172.
(33) Arthur, J. R. Molecular Beam Epitaxy. *Surf. Sci.* **2002**, *500* (1−3), 189−217.
(34) Fu, Z. W.; Wang, Y.; Zhang, Y.; Qin, Q. Z. Electrochemical Reaction of Nanocrystalline Co_3O_4 Thin Film with Lithium. *Solid State Ionics* **2004**, *170* (1−2), 105−109.
(35) Ohnishi, T.; Takada, K. High-Rate Growth of High-Crystallinity $LiCoO_2$ Epitaxial Thin Films by Pulsed Laser Deposition. *Appl. Phys. Express* **2012**, *5* (5), 055502.
(36) Bharathi, K. K.; Tan, H.; Takeuchi, S.; Meshi, L.; Shen, H.; Shin, J.; Takeuchi, I.; Bendersky, L. A. Effect of Oxygen Pressure on Structure and Ionic Conductivity of Epitaxial $Li_{0.33}La_{0.55}TiO_3$ Solid Electrolyte Thin Films Produced by Pulsed Laser Deposition. *RSC Adv.* **2016**, *6* (66), 61974−61983.
(37) Cho, J.; Kim, Y. J.; Park, B. $LiCoO_2$ Cathode Material That Does Not Show a Phase Transition from Hexagonal to Monoclinic Phase. *J. Electrochem. Soc.* **2001**, *148* (10), A1110.
(38) Siller, V.; Gonzalez-Rosillo, J. C.; Eroles, M. N.; Baiutti, F.; Liedke, M. O.; Butterling, M.; Attallah, A. G.; Hirschmann, E.; Wagner, A.; Morata, A.; Tarancon, A. Nanoscaled $LiMn_2O_4$ for Extended Cycling Stability in the 3 V Plateau. *ACS Appl. Mater. Interfaces* **2022**, *14*, 33438−33446.
(39) Julien, C.; Haro-Poniatowski, E.; Camacho-Lopez, M. A.; Escobar-Alarcon, L.; Jimenez-Jarquin, J. Growth of $LiMn_2O_4$ Thin Films by Pulsed-Laser Deposition and Their Electrochemical Properties in Lithium Microbatteries. *Mater. Sci. Eng. B Solid-State Mater. Adv. Technol.* **2000**, *72* (1), 36−46.
(40) Fehse, M.; Trócoli, R.; Hernández, E.; Ventosa, E.; Sepúlveda, A.; Morata, A.; Tarancón, A. An Innovative Multi-Layer Pulsed Laser Deposition Approach for $LiMn_2O_4$ Thin Film Cathodes. *Thin Solid Films* **2018**, *648* (January), 108−112.
(41) Lovett, A. J.; Daramalla, V.; Nayak, D.; Sayed, F. N.; Mahadevegowda, A.; Ducati, C.; Spencer, B. F.; Dutton, S. E.; Grey, C. P.; MacManus-Driscoll, J. L. 3D Nanocomposite Thin Film Cathodes for Micro-Batteries with Enhanced High-Rate Electrochemical Performance over Planar Films. *Adv. Energy Mater.* **2023**, *13*, 2302053.
(42) Lovett, A. J.; Daramalla, V.; Sayed, F. N.; Nayak, D.; de h-Óra, M.; Grey, C. P.; Dutton, S. E.; MacManus-Driscoll, J. L. Low Temperature Epitaxial $LiMn_2O_4$ Cathodes Enabled by NiCo 2 O 4 Current Collector for High-Performance Microbatteries. *ACS Energy Lett.* **2023**, *8*, 3437−3442.
(43) Saccoccio, M.; Yu, J.; Lu, Z.; Kwok, S. C. T.; Wang, J.; Yeung, K. K.; Yuen, M. M. F.; Ciucci, F. Low Temperature Pulsed Laser Deposition of Garnet $Li_{6.4}La_3Zr_{1.4}Ta_{0.6}O_{12}$ Films as All Solid-State Lithium Battery Electrolytes. *J. Power Sources* **2017**, *365*, 43−52.
(44) Pfenninger, R.; Struzik, M.; Garbayo, I.; Stilp, E.; Rupp, J. L. M. A Low Ride on Processing Temperature for Fast Lithium Conduction in Garnet Solid-State Battery Films. *Nat. Energy* **2019**, *4* (6), 475−483.
(45) Mitsuishi, K.; Ohnishi, T.; Tanaka, Y.; Watanabe, K.; Sakaguchi, I.; Ishida, N.; Takeguchi, M.; Ohno, T.; Fujita, D.; Takada, K. Nazca Lines by La Ordering in $La_{2/3-x}Li_{3x}TiO_3$ Ion-Conductive Perovskite. *Appl. Phys. Lett.* **2012**, *101* (7), 073903.
(46) Kim, S.; Hirayama, M.; Cho, W.; Kim, K.; Kobayashi, T.; Kaneko, R.; Suzuki, K.; Kanno, R. Low Temperature Synthesis and Ionic Conductivity of the Epitaxial $Li_{0.17}La_{0.61}TiO_3$ Film Electrolyte. *CrystEngComm* **2014**, *16* (6), 1044−1049.
(47) Wei, J.; Ogawa, D.; Fukumura, T.; Hirose, Y.; Hasegawa, T. Epitaxial Strain-Controlled Ionic Conductivity in Li-Ion Solid Electrolyte $Li_{0.33}La_{0.56}TiO_3$ Thin Films. *Cryst. Growth Des.* **2015**, *15* (5), 2187−2191.
(48) Park, J. S.; Cheng, L.; Zorba, V.; Mehta, A.; Cabana, J.; Chen, G.; Doeff, M. M.; Richardson, T. J.; Park, J. H.; Son, J. W.; Hong, W. S. Effects of Crystallinity and Impurities on the Electrical Conductivity of Li-La-Zr-O Thin Films. *Thin Solid Films* **2015**, *576*, 55−60.
(49) Erinmwingbovo, C.; Siller, V.; Nuñez, M.; Trócoli, R.; Brogioli, D.; Morata, A.; La Mantia, F. Dynamic Impedance Spectroscopy of $LiMn_2O_4$ Thin Films Made by Multi-Layer Pulsed Laser Deposition. *Electrochim. Acta* **2020**, *331*, 135385.
(50) Sastre, J.; Priebe, A.; Döbeli, M.; Michler, J.; Tiwari, A. N.; Romanyuk, Y. E. Lithium Garnet $Li_7La_3Zr_2O_{12}$ Electrolyte for All-Solid-State Batteries: Closing the Gap between Bulk and Thin Film Li-Ion Conductivities. *Adv. Mater. Interfaces* **2020**, *7* (17), 2000425.
(51) Morozov, A. V.; Paik, H.; Boev, A. O.; Aksyonov, D. A.; Lipovskikh, S. A.; Stevenson, K. J.; Rupp, J. L. M.; Abakumov, A. M. Thermodynamics as a Driving Factor of $LiCoO_2$ Grain Growth on Nanocrystalline Ta-LLZO Thin Films for All-Solid-State Batteries. *ACS Appl. Mater. Interfaces* **2022**, *14* (35), 39907−39916.
(52) Lovett, A. J.; Kursumovic, A.; Dutton, S.; Qi, Z.; He, Z.; Wang, H.; MacManus-Driscoll, J. L. Lithium-Based Vertically Aligned Nanocomposite Films Incorporating $Li_xLa_{0.32}(Nb_{0.7}Ti_{0.32})O_3$ electrolyte with High Li^+ ion Conductivity. *APL Mater.* **2022**, *10* (5), 0−7.
(53) Stramare, S.; Thangadurai, V.; Weppner, W. Lithium Lanthanum Titanates: A Review. *Chem. Mater.* **2003**, *15* (21), 3974−3990.
(54) Sun, Y.; Guan, P.; Liu, Y.; Xu, H.; Li, S.; Chu, D. Recent Progress in Lithium Lanthanum Titanate Electrolyte towards All Solid-State Lithium Ion Secondary Battery. *Crit. Rev. Solid State Mater. Sci.* **2019**, *44* (4), 265−282.
(55) Morata-Orrantia, A.; García-Martín, S.; Alario-Franco, M. Á. Optimization of Lithium Conductivity in La/Li Titanates. *Chem. Mater.* **2003**, *15* (21), 3991−3995.
(56) Latie, L.; Villeneuve, G.; Conte, D.; Le Flem, G. Ionic Conductivity of Oxides with General Formula $Li_xLn_{1/3}Nb_{1-x}Ti_xO_3$ (Ln= La, Nd). *J. Solid State Chem.* **1984**, *51* (3), 293−299.
(57) Kim, D. H.; Imashuku, S.; Wang, L.; Shao-Horn, Y.; Ross, C. A. Li Loss during the Growth of (Li, La)TiO_3 Thin Films by Pulsed Laser Deposition. *J. Cryst. Growth* **2013**, *372*, 9−14.
(58) Geohegan, D. B. Imaging and Blackbody Emission Spectra of Particulates Generated in the KrF-Laser Ablation of BN and $YBa_2Cu_3O_{7-x}$. *Appl. Phys. Lett.* **1993**, *62* (13), 1463−1465.
(59) Reimers, J. N.; Dahn, J. R. Electrochemical and In Situ X-Ray Diffraction Studies of Lithium Intercalation in Li_xCoO_2. *J. Electrochem. Soc.* **1992**, *139* (8), 2091−2097.
(60) Xia, H.; Lu, L.; Meng, Y. S.; Ceder, G. Phase Transitions and High-Voltage Electrochemical Behavior of $LiCoO_2$ Thin Films Grown by Pulsed Laser Deposition. *J. Electrochem. Soc.* **2007**, *154* (4), A337.
(61) Inaguma, Y.; Liquan, C.; Itoh, M.; Nakamura, T.; Uchida, T.; Ikuta, H.; Wakihara, M. High Ionic Conductivity in Lithium Lanthanum Titanate. *Solid State Commun.* **1993**, *86* (10), 689−693.

https://doi.org/10.1021/acsenergylett.4c00153
ACS Energy Lett. 2024, 9, 1753−1758